Electronic structure of the strongly-exchange-enhanced paramagnet Ni_3Ga

S. M. Hayden and G. G. Lonzarich
Cavendish Laboratory, University of Cambridge, Cambridge CB3 0HE, United Kingdom

H. L. Skriver
Risø National Laboratory, DK-4000 Roskilde, Denmark

(Received 6 June 1985; revised manuscript received 3 February 1986)

The electronic structure of the incipient ferromagnet Ni_3Ga has been studied by means of the de Haas–van Alphen technique in the magnetic field and temperature ranges $10 \leq H \leq 100$ kG and $0.38 \leq T \leq 4.2$ K, respectively. Concurrently, first-principles energy bands have been calculated by means of the linear-muffin-tin-orbital method. The calculated Fermi surface consists of four concentric hole sheets centered on the point Γ of the simple-cubic Brillouin zone. de Haas–van Alphen frequency branches in close agreement with those expected for *each* of these four sheets have been observed for field directions both in the (100) and (1$\bar{1}$0) planes. The cyclotron masses of these branches, as well as the linear coefficient γ of the electronic heat capacity, are, however, greater than predicted by our band model, by a factor of between 1.5 and 2.7. Comparison of the measured and calculated magnetic susceptibility yields a Stoner enhancement factor of 98, the highest so far reported in an ordered paramagnetic transition metal, and an enhancement of the quadratic coefficient of the inverse susceptibility $\alpha = \partial\chi^{-1}(T)/\partial(T^2)$, of over 8. The strong renormalization of γ and α points to the importance of exchange-enhanced spin fluctuations for this material, as previously reported in the weak itinerant-electron ferromagnet Ni_3Al.

I. INTRODUCTION

Transition metals with very high magnetic susceptibilities at low temperature exhibit a number of striking properties which remain, in many respects, poorly understood. The strong temperature variation of the susceptibility (Fig. 1) and of the nonlinear electronic heat capacity observed, for example, in one such material, Ni_3Ga, seem unlikely to be consistent with the traditional Stoner model, but are also found to be incompatible with the simplest paramagnon and magnetic cluster theories.[1,2] Whether or not more recent magnetic fluctuation models[3–5] can correctly account for these properties in Ni_3Ga is still uncertain.

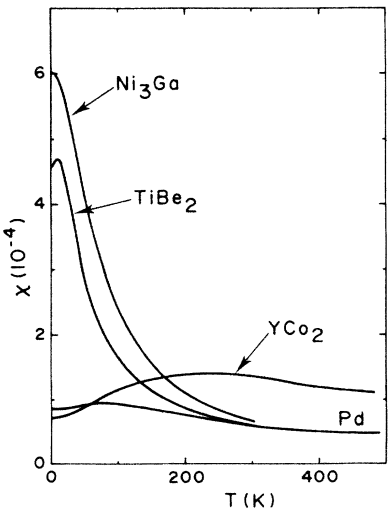

FIG. 1. Temperature dependence of the magnetic susceptibility of Ni_3Ga (Ref. 1) and three other strongly-exchange-enhanced metals $TiBe_2$ (Ref. 21), YCo_2 (Ref. 22), and Pd (Ref. 23). (The magnetic susceptibility is in Gaussian units.)

To perform realistic quantitative tests of theory we require detailed information on the electronic structure near the Fermi level ε_F, and on the low-lying magnetic excitation spectrum. To provide a part of the necessary information we have investigated the Fermi surface and cyclotron masses in Ni_3Ga by the de Haas–van Alphen (dHvA) technique and calculated the band structure by the linear-muffin-tin-orbital (LMTO) method in the local-spin-density (LSD) approximation. Our study sheds light on the accuracy of a first-principles band calculation near ε_F in a metal on the verge of ordering ferromagnetically at low temperature, and makes possible the construction of an accurate semi-empirical band model which may be used to calculate the thermal properties in terms of the conventional Stoner model and, with greater computational effort, in terms of more sophisticated magnetic fluctuation theories.

Ni_3Ga crystallizes in the simple-cubic Cu_3Au ($L1_2$) structure and may be prepared in a highly homogeneous and ordered state by a technique similar to that originally developed for Ni_3Al.[6] The dHvA spectra observed in our purest samples consist of up to 12 frequency components. Four fundamental frequency branches can be unambiguously identified, by their angular variation and magnitude, with principal orbits on the four concentric hole sheets of the Fermi surface, 14, 15, 16, and 17, predicted by the LMTO model. In high magnetic fields, branches associat-

ed with sheets 14 and 15 exhibit a splitting which can be well understood in terms of the effect of the spin-orbit interaction and the strongly enhanced Zeeman splitting of the bands. The effect of the field-induced exchange splitting on the branches associated with sheets 16 and 17 is not fully resolved by the present investigation.

Experimental and calculated frequencies agree to a precision corresponding to better than 3 mRy in the position of the bands near ε_F, for all four bands. However, the cyclotron masses are systematically higher than predicted by our model, by a factor varying between 1.5 and 2.6 for the different bands. As discussed in Sec. V these values are consistent with the ratio of the measured and the band calculated linear coefficient γ of the heat capacity.

The observed magnetic susceptibility $\chi(T)$ is also much stronger than predicted by the band model in its simplest form. In particular, the ratio of the measured and calculated values of $\chi(0)$ and of $\alpha=\partial\chi^{-1}(0)/\partial(T^2)$ are found to be 98 and over 8, respectively. The large (Stoner) enhancement of $\chi(0)$ can perhaps be understood in terms of our band model, if calculated self-consistently in the presence of a finite field H. However, the enhancements of the thermal coefficients γ and α lie outside the framework of this model and point to the importance of coherent spin fluctuations as previously established in the related weak itinerant ferromagnet Ni_3Al.[7,4,5]

II. EXPERIMENTAL RESULTS

Single-crystal samples of Ni_3Ga were prepared by a technique similar to that described by Bernhoeft *et al.*[6] Nickel rods (Johnson Matthey spectroscopically pure grade) were zone refined to achieve purity levels corresponding to residual resistivity ratios [ρ(293 K)/ρ(4.2 K)] in excess of 2000. The gallium (Johnson Matthey puratronic grade) had a residual resistivity ratio in excess of 10 000. The constituents were thoroughly mixed and homogenized by mechanical stirring at approximately 1550 °C in a carefully cleaned alumina crucible. Small losses of gallium due to evaporation were compensated by corrected amounts of starting material. The melt was quenched in the homogeneous state and subsequently annealed for four days at a series of temperatures below the peritectic temperature to promote grain growth and a high degree of chemical ordering. The resulting ingots, which possessed single-crystal grains up to 6 mm across, were characterized by resistivity measurements, electron-beam microanalysis, x-ray diffraction, and mass spectrometry. The best specimen had a residual resistivity ratio of 76 and exhibited no evidence (from the above-mentioned characterization studies) of microprecipitates or high mechanical strains. Single-crystal disks 3 mm in diameter and 0.5 mm thick with their planes normal to the [110] or [100] directions, were prepared by low-power spark erosion followed by deep chemical polishing to remove surface damage and to produce smooth surfaces. Measurements were carried out both in the best specimens described above and in one sample with a residual resistivity ratio about an order of magnitude lower. In the latter, only frequencies arising from sheets 14 and 15 could be observed, the values of which were comparable to those studied in detail in the best samples. Only results for the purest [110] and [100] samples are presented in this paper.

The dHvA magnetization was detected by means of a field modulation technique employing low modulation frequencies and high amplitudes, both adjusted to maximize signal to noise. Details of the technique are given elsewhere.[8,9] and here we summarize only key points. A superconducting magnet, with a homogeneity of one part in 10^5 over a 15-mm-diam spherical volume, generated a magnetic field of up to 87 kG when cooled to 4.2 K and approximately 100 kG when at 1.8 K, and a ^{3}He cryostat provided temperatures as low as 0.38 K. Most measurements were carried out with a modulation frequency of 117 Hz and detection was at the second or fourth harmonic. The modulation amplitude was varied up to a maximum of 300 G to optimize signal to noise and, where necessary, to filter unwanted signals. The quasistatic magnetic induction $B=H+4\pi(1-D)M$ was determined from the applied field H, calibrated by an NMR spectrometer, the known demagnetizing factor D, and the magnetization $M(T,H)$ of the sample. Corrections to B due to $M(T,H)$ are small but, because of the strong exchange enhancement of the susceptibility, could not be neglected in the experimental field range. Corrections due to magnetic anisotropy may be estimated from experimental measurements in Ni_3Al,[7,10] and are expected to be small and insignificant. dHvA frequencies (F) and thus the corresponding extremal cross-sectional areas of the Fermi surface ($A=2\pi eF/\hbar c$) were derived from on-line computations of the amplitude spectra averaged over increasing and decreasing field sweeps. The amplitude spectrum is here defined as the square root of the sum of the squares of the real and imaginary parts of the Fourier transform of the data multiplied by a Hanning window. Zeros were padded in the fast-Fourier-transform technique to increase the density of points for accurate amplitude and frequency determinations. Fundamental components were distinguished from harmonics and combination frequencies by a careful study of the orientation and temperature dependence of the spectra. Typical spectra with both fundamental and harmonic components are presented in Figs. 2, 3, and 4 and the orientation dependence of the fundamental frequency branches are given in Fig. 5. The absolute accuracy of the fundamental frequencies (labeled by Greek letters) is better than $\pm 3\%$. This maximum uncertainty is due to residual interference of neighboring frequencies and the effects of the field dependence of the amplitude and frequency in the field range of the measurements.

The measured frequency is in general related to the true frequency F by $(H/B)^2(dB/dH)(F-B\,dF/dB)$.[7] We correct for the factor $(H/B)^2(dB/dH)$ so that *the frequencies given in this paper represent the quantity* $(F-B\,dF/dB)\simeq(F-H\,dF/dH)$. At low fields this reduces to the value of F in the zero-field limit. At the highest fields which we have investigated, the difference between the measured and the low-field value of F is estimated, from earlier measurements in Ni_3Al,[7] to be as high as perhaps $\pm 3\%$, and thus is comparable to the earlier given overall uncertainty. The field dependence of the

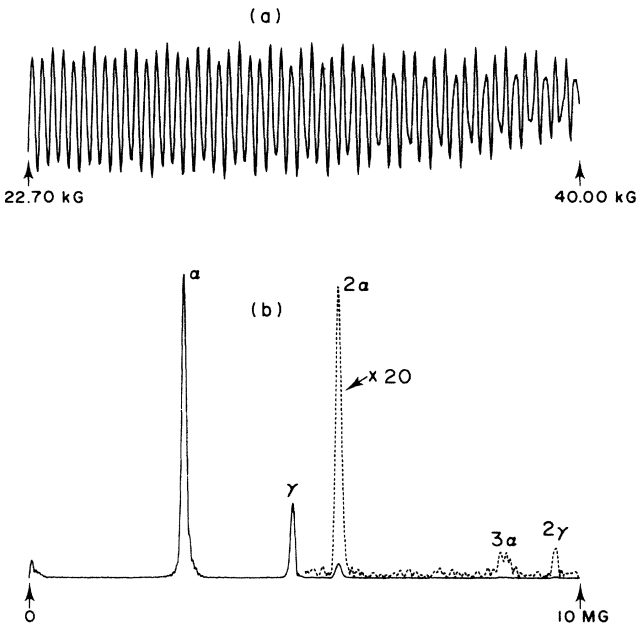

FIG. 2. Typical (a) dHvA oscillations and (b) amplitude spectrum in Ni_3Ga at 0.40 K in the [001] field orientation and in the field range $22.70 \leq H \leq 40.00$ kG. The spectrum (uncorrected in this and in the following two figures for slight instrumental shifts) consists of the fundamental α and γ frequencies and their harmonics.

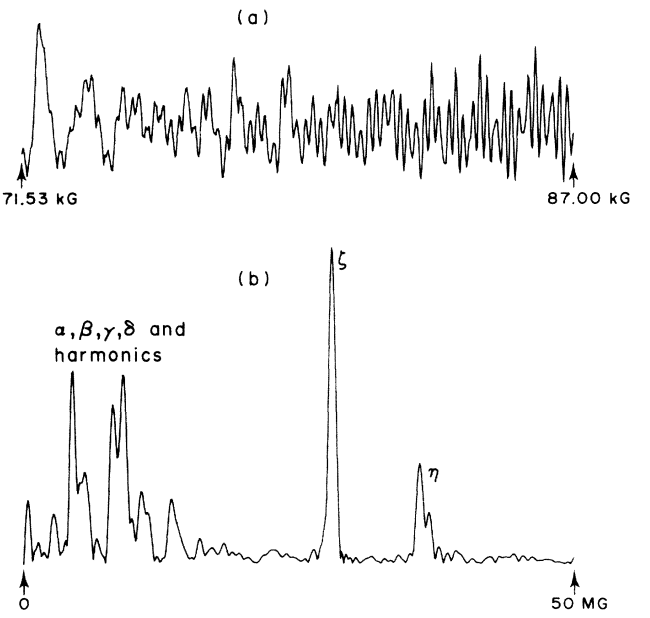

FIG. 4. Typical (a) dHvA oscillations and (b) amplitude spectrum at 0.44 K in the [001] field orientation and in the field range $71.53 \leq H \leq 87.00$ kG. The spectrum consists of the ζ and η frequencies and a large number of incompletely resolved peaks associated with the α, β, γ, and δ frequencies and their harmonics. The small splitting of the η frequency is discussed in Sec. IV B.

frequencies associated with sheets 14 and 15, in particular, will be discussed in Sec. IV B.

Cyclotron masses were determined along the principal symmetry directions from the temperature dependence of the dHvA amplitudes. The experimental details and the precautions taken in the execution of these measurements are described by Sigfusson *et al.*[7] The accuracy of mass measurements is better than $\pm 6\%$ and is entirely governed by the accuracy with which the sample temperature can be determined in liquid ^{3}He. As in the earlier

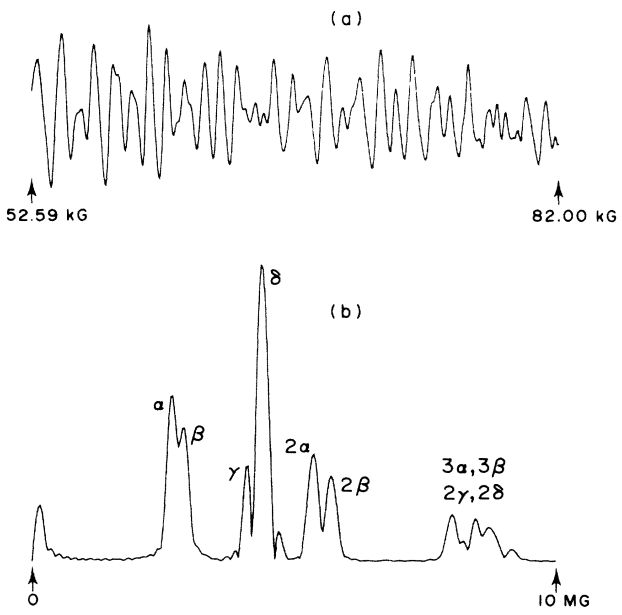

FIG. 3. Typical (a) dHvA oscillations and (b) amplitude spectrum at 0.40 K in the [111] field orientation in the field range $52.59 \leq H \leq 82.00$ kG. The fundamental α and γ frequencies in Fig. 2 split, in high fields, into two pairs labeled α,β and γ,δ, respectively.

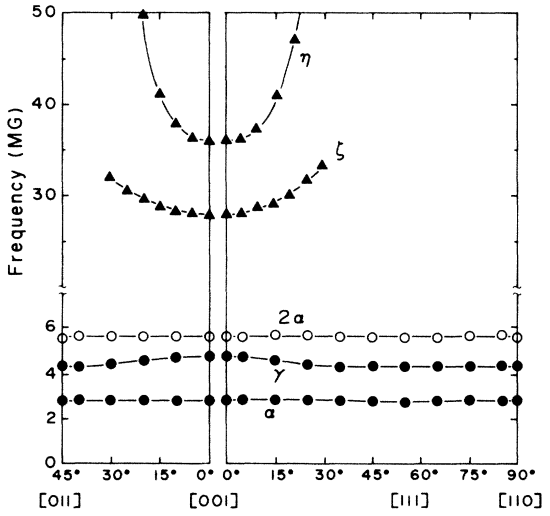

FIG. 5. Variation of the fundamental frequency branches (●,▲), and the dominant harmonic branch (○), for field orientations in both the $(1\bar{1}0)$ and (100) planes. Measurements were made at 0.40 K in the field range $31.1 \leq H \leq 40.0$ kG (for the α and γ branches) and $79 \leq H \leq 84$ kG (for the ζ and η branches). The solid lines serve to connect data points on the same branch. Fine structure due to the field-induced exchange splitting was, in these measurements, unresolved (see Sec. IV B). The experimental uncertainty of the frequencies is discussed in Sec. II.

work the temperature was measured with a calibrated carbon thermometer with a low thermal mass and high surface area, placed close to the sample. In parallel the temperature was also checked by vapor-pressure thermometry corrected for hydrostatic pressure and the thermomolecular effect. Control measurements for the low-mass orbits were also carried out in liquid ^{4}He. As pointed out by Lonzarich[11] (see also Lonzarich and Gold[12]), the overall dHvA magnetization in ferromagnetic or nearly ferromagnetic metals may contain a contribution at high fields from *oscillations in the spin part of the total magnetic moment.* This effect has also been reexamined by Gunn[13] in connection with possible field-induced instabilities in very strongly enhanced paramagnetic metals. Spin oscillations may be expected to alter the field dependence of the amplitude but should not affect the fundamental frequencies or the cyclotron masses, which are the focus of our present attention.

III. BAND-STRUCTURE CALCULATIONS

The energy-band structure has been evaluated by means of the linear-muffin-tin-orbital (LMTO) technique[14] employing the von Barth-Hedin approximation[15] for the local exchange correlation potential. The self-consistent calculations are based on a lattice constant of $a=3.575$ Å for the Ni_3Ga unit cell (Fig. 6), and include s, p, and d partial waves and corrections to the atomic sphere approximation. Energy eigenvalues are determined at 286 points in a uniform mesh in the $\frac{1}{48}$th irreducible wedge of the simple-cubic Brillouin zone (Fig. 6).

The energy bands obtained along the directions of high symmetry without the spin-orbit interaction are shown in Fig. 7. The calculated central sections of the Fermi surface both with and without spin-orbit are presented in Figs. 8(a) and 8(b), respectively. Four bands, 14, 15, 16, and 17, of predominant d character, cross the Fermi level and give rise to the four hole sheets of the Fermi surface centered on Γ with the corresponding labels in Figs. 8(a) or 8(b). Sheets 14 and 15 are concentric nearly spherical pockets which are strongly hybridized by the spin-orbit interaction [Fig. 8(b)]. Sheet 16 is a large closed surface

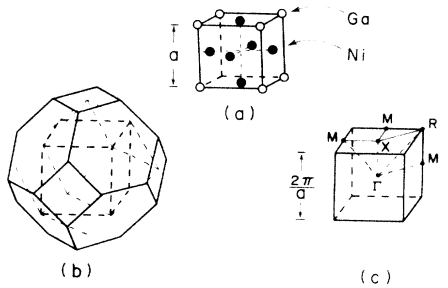

FIG. 6. (a) Unit cell of the Ni_3Ga simple-cubic ($L1_2$) crystal structure: ●, Ni; ○, Ga, $a=3.58$ Å. (b) The first four Brillouin zones of the simple-cubic lattice; the outer boundary of the third zone is not shown. (c) Symmetry labels for the first Brillouin zone of the simple-cubic crystal lattice.

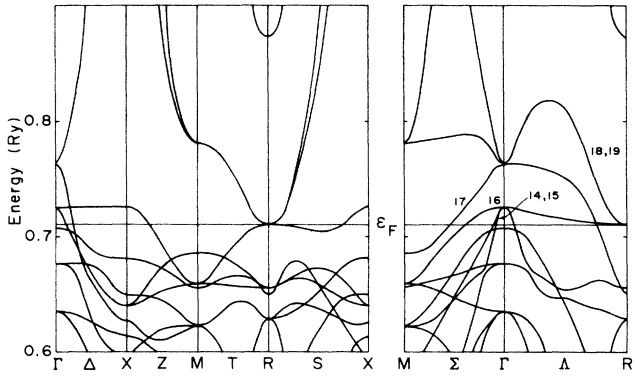

FIG. 7. Energy bands near the Fermi level calculated by the model described in Sec. III. The calculations are self-consistent and relativistic but without the spin-orbit interaction. The wave functions associated with bands 14 to 17, which cross the Fermi level, contain strong contributions from the d orbitals of the Ni atoms.

with arms extending along the ⟨111⟩ directions. Sheet 17 is a large open surface with arms along ⟨111⟩ and necks extending along the ⟨100⟩ directions. In the absence of spin-orbit coupling, bands 18 and 19 also just cross the Fermi level to produce tiny electron pockets centered on

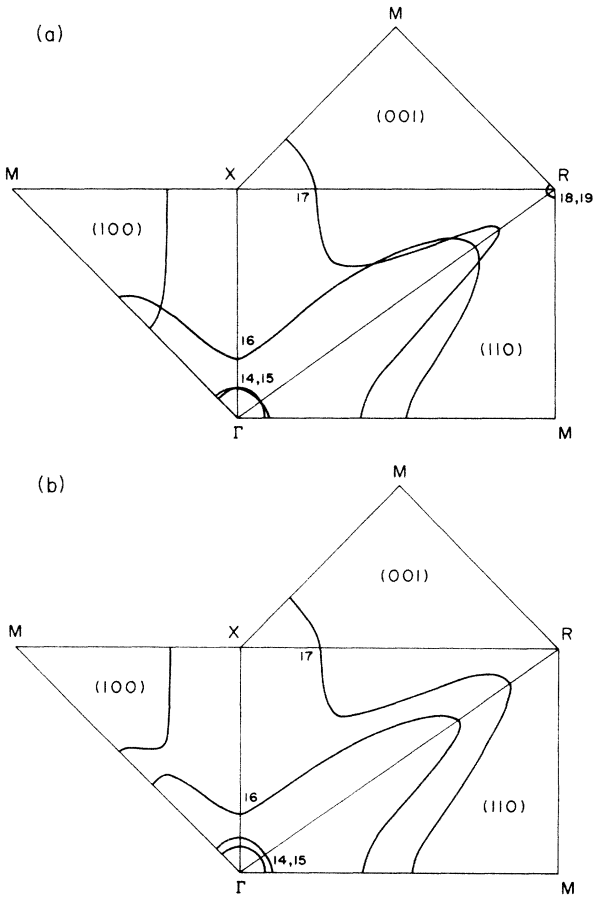

FIG. 8. Principal sections through the Fermi surface calculated by the model described in Sec. III, (a) without and (b) with the spin-orbit interaction.

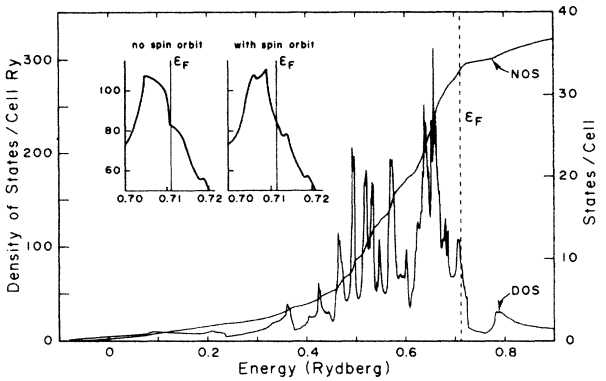

FIG. 9. Density of states (states per Ry per molecule for both spins) calculated by the model of Sec. III without the spin-orbit interaction. The left and right expanded views in the insets are without and with spin orbit, respectively. The density of states N_F per Ry per spin per average atom at ϵ_F is 10.3 without spin orbit and 10.6 with spin orbit.

the R point of the Brillouin zone. These pockets are very sensitive to the precise form of the lattice potential and are suppressed entirely in our model when spin-orbit coupling is included.

Finally, we have calculated the overall electronic density of states both with and without spin-orbit coupling and the results are presented in Fig. 9. Our band structure for Ni_3Ga is very similar to that calculated by Skriver (see Ref. 10) and Buiting *et al.*[16] for the hypothetical spin unpolarized state of Ni_3Al, but is *very markedly* different from that of Fletcher[17] for Ni_3Ga itself in which only two bands cross the Fermi level. These bands give rise to two Γ-centered hole surfaces, only one of which can be unambiguously related to any of the four sheets obtained in our calculation. One of the aims of our dHvA study is to distinguish between these strikingly different predictions for the Fermi surface.

IV. EXPERIMENTAL RESULTS AND THEIR INTERPRETATION

A. Paramagnetic Fermi surface and cyclotron masses

The fundamental frequency branches observed for field orientations in both the $(1\bar{1}0)$ and (100) planes are plotted in Fig. 5. Frequencies along the principal symmetry directions and their corresponding masses are summarized and compared with the predictions of our band model in Table I. The two lowest branches α and γ have masses in the range of 0.4 to $0.7m_0$, are nearly isotropic, and can be detected in all field orientations investigated. Their magnitudes and angular variations are consistent with the existence of two quasispherical pockets of the Fermi surface which are very similar to our calculated sheets 14 and 15, to which these branches are accordingly assigned. The ζ branch, which has a mass of $5.5m_0$ (at [001]), is observed within an angular range of 30° around [001] and varies roughly as $1/\cos\theta$ as expected for a cylindrical surface. Both its magnitude and anisotropy clearly identifies this branch with the X-centered necks of sheet 17. Finally, the η branch, which has a mass of $3.6m_0$ (at [001]), is observed over a range of approximately 20° around [001] and varies more rapidly than $1/\cos\theta$ as expected for a fluted or hyperboloidal surface. Both the magnitude and anisotropy of this branch lead us to identify it with the Γ-centered waist of sheet 16. These identifications of the four experimental branches are illustrated in Fig. 10, which presents three-dimensional perspectives of the calculated sheets of the Fermi surface.

A detailed comparison of measured and predicted branches is given in Fig. 11. In view of the fact that our calculations involve no adjustable parameters, the overall level of agreement between theory and experiment is remarkably good. We conclude that our band model, in contrast, for example, to that of Fletcher[17] discussed in Sec. III, provides a realistic first-order description of characteristic parts of the Fermi surface of Ni_3Ga.

TABLE I. Summary of experimental and calculated frequencies and cyclotron masses at symmetry directions. The measurements were carried out in the field and temperature ranges $31 \le H \le 40$ kG and $0.42 \le T \le 1.4$ K, respectively, for the α and γ branches, and $79 \le H \le 84$ kG and $0.39 < T < 0.85$ K, respectively, for the ζ and η branches. The calculations of the frequencies and of the masses in column A are based on the band structure of Sec. III with the spin-orbit interaction. Cyclotron masses under column B were calculated with this band structure adjusted slightly, by a rigid shift of each band, to yield extremal areas in agreement with experiment. [Conversion of frequency in MG to area in atomic units is given by $A(\text{a.u.}) = 2.673 \times 10^{-3} F(\text{MG})$.]

			Frequency (MG)		Cyclotron masses (m_0)			
						Calc.		
Orientation	Branch	Orbit	Expt.	Calc.	Expt.	A	B	Expt./Calc. (B)
[001]	α	Γ_{14}	2.83(5)	3.40	0.54(2)	0.32	0.28	1.9
	γ	Γ_{15}	4.71(8)	5.87	0.71(2)	0.47	0.42	1.7
	ζ	X_{17}	27.7(3)	26.8	5.5(3)	2.1	2.1	2.6
	η	Γ_{16}	36.1(6)	41.1	3.7(2)	2.2	2.1	1.8
[111]	α	Γ_{14}	2.73(5)	3.32	0.40(2)	0.31	0.27	1.5
	γ	Γ_{15}	4.27(8)	5.33	0.65(2)	0.41	0.37	1.8
[110]	α	Γ_{14}	2.85(5)	3.40	0.55(2)	0.32	0.29	1.9
	γ	Γ_{15}	4.36(8)	5.30	0.68(2)	0.39	0.35	1.9

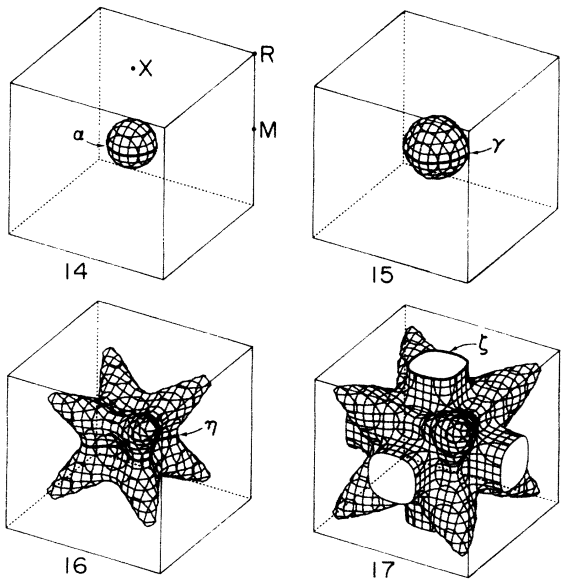

FIG. 10. Perspective views of the four sheets of the Fermi surface, the principal sections of which are presented in Fig. 8(b). The bold solid lines illustrate the central cyclotron orbits responsible for the four fundamental dHvA frequencies α, γ, ζ, and η observed for field directions near [001]. Sheets 14 and 15 have been expanded for clarity.

As seen from Table I, however, the measured cyclotron masses are larger than predicted by our model for all four sheets of the Fermi surface. This pronounced mass enhancement, which is characteristic of ferromagnetic or nearly ferromagnetic metals in general,[4,18] is between 1.5 and 1.9 for sheets 14, 15, and 16, and as high as 2.6 for the necks of sheet 17.

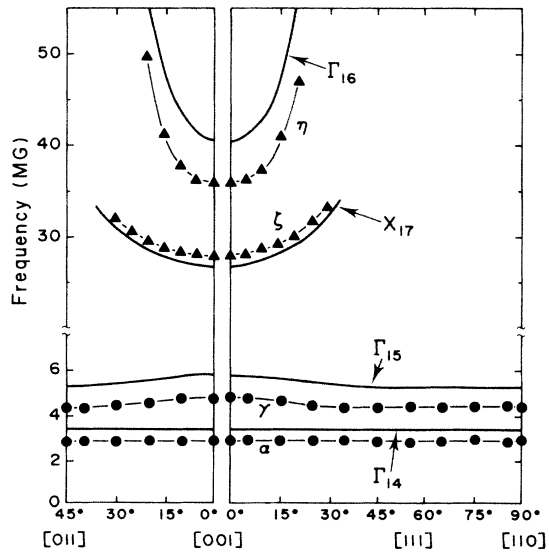

FIG. 11. Variation of observed (●,▲) and calculated (bold solid lines) fundamental dHvA frequencies in the $(1\bar{1}0)$ and (001) planes. Calculations were done with the model described in Sec. III including the spin-orbit interaction. (The thin lines serve only to connect data points on the same branch).

The α, γ, and ζ branches in Ni_3Ga are very similar both in topology and magnitude, to the branches with the same labels observed in the weak ferromagnet Ni_3Al.[7] The η oscillations, which we observed only in the very purest Ni_3Ga samples under optimum experimental conditions, were not detected in Ni_3Al. We note that the mass enhancement in Ni_3Al is somewhat higher than in Ni_3Ga but exhibits a similar anisotropy. In particular, the enhancement in both materials is much higher for the necks of sheet 17 (2.6 for Ni_3Ga and approximately 3 for Ni_3Al) than for the spherical sheets 14 and 15 (typically 1.7 for Ni_3Ga and 2.0 for Ni_3Al).

B. Field-induced exchange splitting

In this section we discuss the field-induced exchange spitting of sheets 14 and 15 which may be contrasted with the stronger spontaneous splitting observed for the corresponding sheets in Ni_3Al (Fig. 12). As shown in this figure, in the low-field limit where the field-induced splitting of the Fermi surface of Ni_3Ga may be neglected, sheets 14 and 15 give rise to two sharp peaks in the dHvA spectrum whose separation is determined primarily by the spin-orbit interaction. In higher magnetic fields in Ni_3Ga, and for any field in the ferromagnetic state of Ni_3Al, the Kramer degeneracy of these peaks is lifted and the average separa-

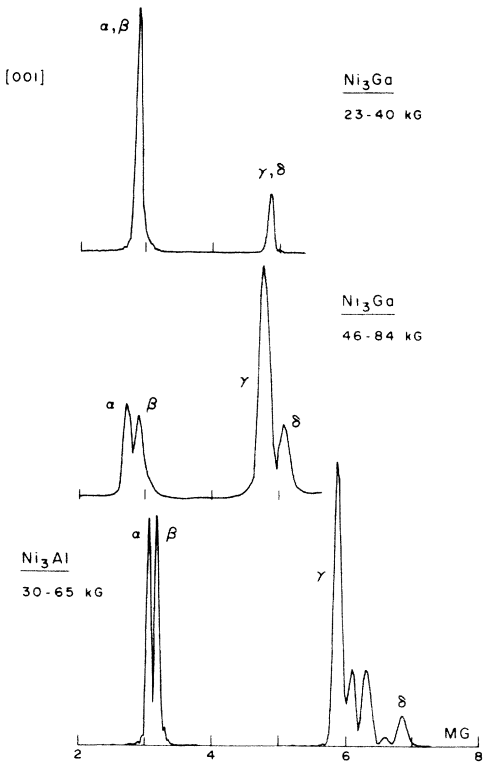

FIG. 12. Effects of spin orbit (top trace) and spin orbit and exchange (middle and bottom traces) on the [001] dHvA amplitude spectra arising from quasidegenerate sheets 14 and 15 of the Fermi surfaces of Ni_3Ga and Ni_3Al (Ref. 7). The horizontal scale (frequency in MG) is the same for all three traces. (The spectra are not corrected for small instrumental frequency shifts.)

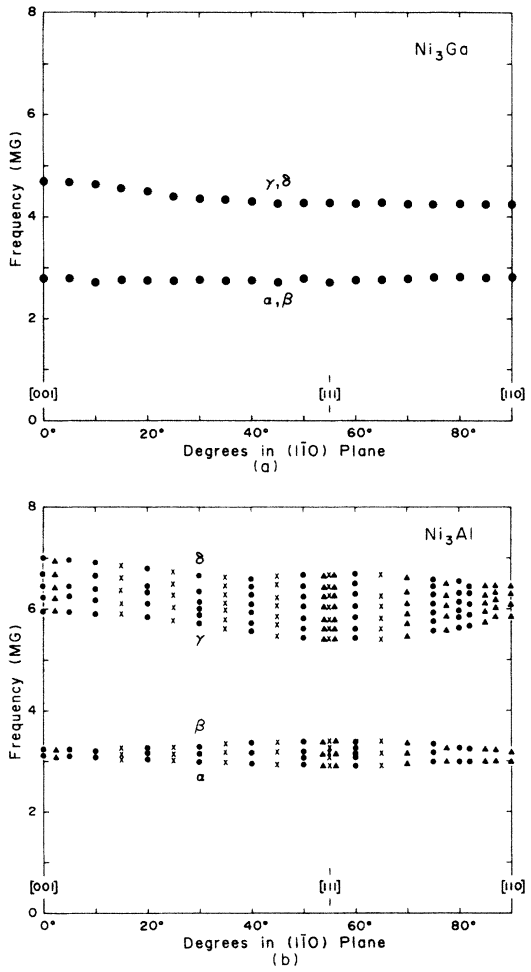

FIG. 13. Comparison of (1$\bar{1}$0) frequency branches due to the quasidegenerate sheets 14 and 15 (a) in Ni_3Ga and (b) in Ni_3Al (Ref. 7). The Kramers degeneracy of the α,β and of the γ,δ branches in Ni_3Ga at low fields is lifted by the finite exchange splitting in the ferromagnetic state of Ni_3Al. The intermediate branches in Ni_3Al are due to magnetic breakdown (Ref. 7).

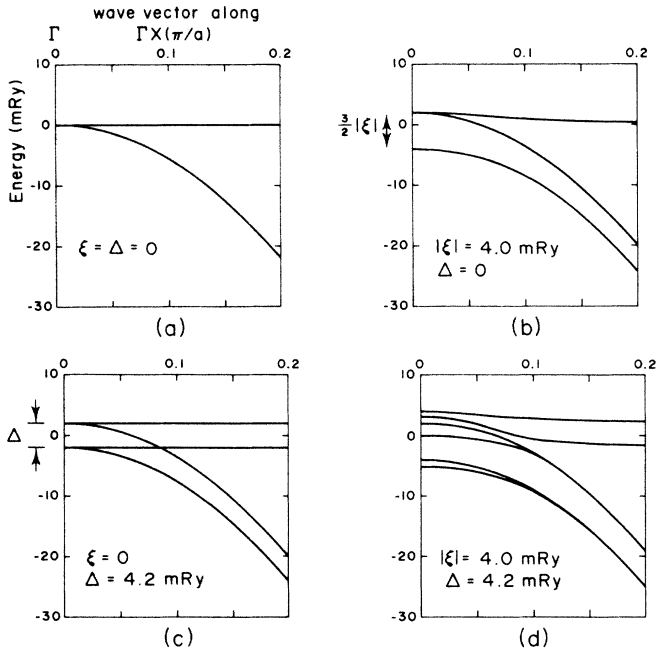

FIG. 14. Expanded views of bands 14, 15, and 17 near ε_F and along ΓX in the simple-cubic Brillouin zone, for different values of the spin-orbit parameter ξ and exchange splitting Δ: (a) $\xi=\Delta=0$; (b) $|\xi|=4.0$ mRy, $\Delta=0$; (c) $\xi=0$, $\Delta=4.2$ mRy; and (d) $|\xi|=4.0$ mRy, $\Delta=4.2$ mRy ($\mathbf{M}\perp\Gamma X$). Calculations are based on a $\mathbf{k}\cdot\mathbf{p}$ model (Ref. 7), the basic parameters of which were derived from a fit to the band structure described in Sec. III. The fitted spin-orbit parameter ξ is approximately 70% of the atomic value for Ni. The exchange splitting Δ in (b) and (d) was taken to be $(n_\uparrow-n_\downarrow)/N_F$, where $n_\uparrow-n_\downarrow$ is the unpaired number of electrons per average atom and N_F is the calculated density of states of ε_F per spin per average atom. N_F was set to 10.6 $Ry^{-1}spin^{-1}$(average atom)$^{-1}$ (Fig. 9) and $n_\uparrow-n_\downarrow$ to 0.045 (average atom)$^{-1}$, i.e., the empirical value for H near 65 kG (Ref. 19).

tion of the peaks is increased by the exchange field. The change of branches α,β and γ,δ from the low-field paramagnetic state of Ni_3Ga to the spin-polarized state of ferromagnetic Ni_3Al is shown in Figs. 13(a) and 13(b).

The Ni_3Al branches in Fig. 13(b) have been analyzed in terms of a $\mathbf{k}\cdot\mathbf{p}$ model Hamiltonian including the off-diagonal spin-orbit and diagonal exchange interactions by Sigfusson *et al.*[7] Calculated [001] cross-sectional areas in this model accounted well for the observed frequencies in terms of realistic values of the spin-orbit parameter and the exchange splitting. We note that the large number of intermediate branches in Fig. 13(b) have been explained in terms of magnetic breakdown between the fundamental α and β and γ and δ orbits.[7]

The above $\mathbf{k}\cdot\mathbf{p}$ model has also been used to determine the effects of spin orbit and exchange on sheets 14 and 15 for parameters appropriate to Ni_3Ga, and the results are presented in Figs. 14 and 15. The magnitude of the spin-orbit parameter ξ was determined from our band structure

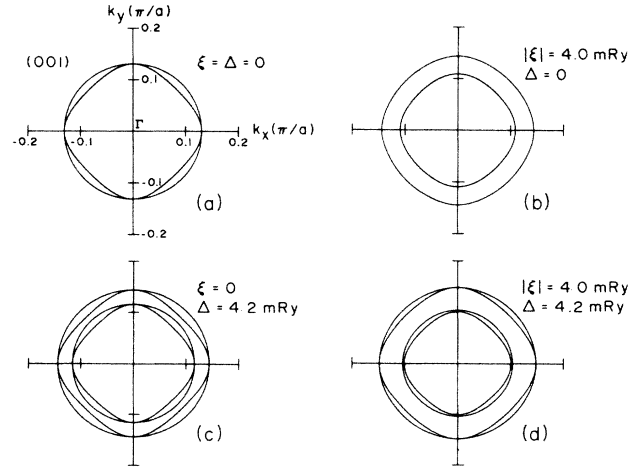

FIG. 15. (001) central cross sections of the Fermi surface near Γ calculated by means of the $\mathbf{k}\cdot\mathbf{p}$ band model of Fig. 14: (a) $\xi=\Delta=0$; (b) $|\xi|=4.0$ mRy, $\Delta=0$; (c) $\xi=0$, $\Delta=4.0$ mRy; and (d) $|\xi|=4.0$ mRy, $\Delta=4.2$ mRy, ($\mathbf{M}$ along [001]). (b) and (d) give the expected cross sections for $\mathbf{H}$ parallel to [001] and H equal to 0 and about 65 kG, respectively.

of Sec. III to be approximately 4.0 m Ry at the top of the d bands, i.e., about 70% of the atomic value for Ni. The exchange splitting in the $\mathbf{k}\cdot\mathbf{p}$ model was taken to be $(n_\uparrow - n_\downarrow)/N_F$, where $(n_\uparrow - n_\downarrow)$ is the measured number of spin unpaired carriers per average atom, and N_F is the calculated density of states per spin per average atom. The calculations in Figs. 14(b), 14(d), and 15(b), 15(d) assume $n_\uparrow - n_\downarrow$ to be 0.045 (average atom)$^{-1}$, i.e., the experimental value at 65 kG,[19] and N_F to be 10.6 Ry^{-1}spin^{-1}(average atom)$^{-1}$, that is, the value calculated with spin-orbit coupling (Fig. 9). The position of bands 14 and 15 relative to ε_F was adjusted slightly to fit closely the observed dHvA frequencies at [001] in the low-field limit.

As shown in Figs. 14(b), 14(d), and 15(b), 15(d) the Fermi surface for bands 14 and 15 is expected to change significantly within the field range of our experiments. The corresponding changes in the measured dHvA frequencies $F - H\partial F/\partial H$ are, however, less pronounced. At 65 kG a splitting of about 5% is predicted by our $\mathbf{k}\cdot\mathbf{p}$ model for both the lower (α,β) and upper (γ,δ) frequencies at [001], which is consistent, to the experimental error, with observation (Fig. 12). We note that in Ni_3Al, in contrast to Ni_3Ga, the splitting of the lower branch was calculated to be much smaller than that for the upper branch. As shown in Figs. 12 and 13, this prediction is well supported by the experimental results.

The exchange field is, of course, also expected to lift the spin degeneracy of the branches associated with sheets 16 and 17 which, like 14 and 15, have a strong d character. Two very close branches unambiguously associated with sheets 16 are in fact observed (Fig. 3, η), however, only one branch (Fig. 3, ζ) has been seen which can clearly be identified with sheet 17. Thus in this case the spin splitting of the dHvA frequency is anomalously small or the amplitude of one of the spin split branches is unusually weak. An absence of a detectable splitting or of a companion frequency for the ⟨100⟩ neck of sheet 17 was also reported for Ni_3Al.[7] Measurements at higher magnetic field may help clarify this unexpected finding.

V. ENHANCEMENT OF THE ELECTRONIC HEAT CAPACITY AND THE MAGNETIC SUSCEPTIBILITY

In this section we compare experimental values of parameters of the low-temperature magnetic equation of state and heat capacity of Ni_3Ga with those calculated in the traditional one-particle model, using the band structure of Sec. III which gives a good account of the dHvA frequency spectra.

In the one-particle model the magnetic equation of state $M = M(T,H)$ is, for a low applied field H and temperature T, given by

$$H = a_0 M + b_0 M^3 + \cdots , \tag{1}$$

where

$$a_0 = \chi_0^{-1} + \alpha_0 T^2 + \cdots , \tag{2}$$

$$\chi_0 = g^2 \mu_B^2 N_a N_F / 2V , \tag{3}$$

$$\alpha_0 = \pi^2 k_B^2 (\nu_1^2 - \nu_2)/6\chi_0 , \tag{4}$$

and

$$b_0 = \mu_B^2 (\nu_1^2 - \nu_2/3)/2\chi_0^3 + \cdots . \tag{5}$$

N_a is the total number of atoms, V is the volume, N_F is the density of states per spin per average atom at ε_F, $\nu_1 = N_F'/N_F$, $\nu_2 = N_F''/N_F$, where N_F' and N_F'' are, respectively, the first and second energy derivatives of N_F at ε_F, g is the spectroscopic splitting factor, and μ_B is the Bohr magneton (see Lonzarich and Taillefer[5] for a recent discussion of the magnetic equation of state in nearly or weakly ferromagnetic metals). In the same model the electronic heat capacity at low temperatures is of the form

$$C = \gamma_0 T + \cdots , \tag{6}$$

where

$$\gamma_0 = 2\pi^2 k_B^2 N_a N_F / 3 , \tag{7}$$

and k_B is the Boltzmann factor.

Values of χ_0, γ_0, b_0, and α_0, calculated using the band-structure parameters given in Table II, are presented in the third column of Table III. Over a limited range in temperature and field the empirical magnetic equation of state and (to a lesser extent) the heat capacity can be interpreted approximately in terms of Eqs. (1), (2), and (6) but with effective parameters χ, γ, b, and α replacing χ_0, γ_0, b_0, and α_0, respectively. The experimental values of χ, γ, and α, given in column 2 of Table III, are all higher, and for χ and α much higher, than the calculated values.

The large enhancement of the $T=0$ susceptibility, i.e., the large Stoner factor $S = \chi/\chi_0 \simeq 98$, may perhaps be understood in terms of our band model if made self-consistent in the presence of a finite magnetic field. Such an analysis would lead principally to a replacement of a_0 by $a = a_0 - \lambda = a_0/S$ in Eq. (1). This replacement yields an equation of state of the form expected in Stoner's mean-field theory, in which the one-particle energies are spin spilt by an effective field equal to the applied field plus the molecular field λM proportional to the magnetization. In this Stoner model, however, the remaining parameters γ_0, b_0, and α_0 are essentially unaffected.

To interpret the large enhancement of the linear coefficient γ of the heat capacity and cyclotron masses m_c^*

TABLE II. Parameters used in the calculations of Sec. V (Table III). N_F is the density of states at the Fermi energy and N_F' N_F'' are, respectively, the first and second energy derivatives of N_F, calculated by means of the band model of Sec. III with the spin-orbit interaction.

Parameters	Ni_3Ga
V/N_a	11.5[a] Å^3 (average atom)$^{-1}$
g	2[b]
N_F	10.6 states Ry^{-1}spin^{-1}(average atom)$^{-1}$
$\nu_1 = N_F'/N_F$	-66 Ry^{-1}
$\nu_2 = N_F''/N_F$	>0[c] Ry^{-2}

[a]Assuming a lattice constant of 3.58 Å (Fig. 6).
[b]The orbital correction is not known but is expected to be unimportant for the present calculations.
[c]ν_2 is positive but its magnitude cannot be reliably determined from our density of states.

TABLE III. Comparison of experimental and band-calculated values of the low-temperature magnetic susceptibility χ, the linear coefficient of the heat capacity γ, the cubic coefficient $b=\partial H/\partial(M^3)$ of the magnetic equation of state, and the quadratic coefficient $\alpha=\partial\chi^{-1}/\partial(T^2)$ of the inverse susceptibility. The calculations are based on the parameters in Table II, unless otherwise stated. We observe that the enhancement of γ is comparable to that of the cyclotron masses given in Table I.

Parameters	Expt.	Calc.	Expt./Calc.
χ (10^{-4})	7.14[a]	0.073	98
γ [mJ K^{-2} (mole average atom)$^{-1}$]	9.9[b]	3.7	2.7
	6.0[c]	3.7	1.6
b (G^{-2})	0.33[a]	<1.0[d]	>0.33[f]
α (K^{-2})	0.34[a]	<0.040[d]	>8.5[f]
		<0.015[d,e]	>23[f]

[a]Reference 1; χ and b are obtained from extrapolation to zero H and T of magnetization data obtained in high magnetic fields (up to 350 kG).
[b]Reference 2; based on analysis of heat-capacity data in the temperature range $1\leq T\leq 5$ K and in zero applied magnetic field.
[c]As in footnote b, but based on analysis of heat-capacity data in the higher-temperature range $10\leq T\leq 15$ K.
[d]The inequality is due to the condition $\nu_2>0$.
[e]Assuming that $\nu_2>0$ (Table I) and that ν_1 is given by Eq. (5) with b_0 set equal to the experimental value of 0.33 G^{-2} (footnote a).
[f]Assuming that the calculated value is positive.

(Table I), and the even larger enhancement of the quadratic coefficient α of the inverse susceptibility, it is necessary to take account of residual interactions of thermally excited particles and holes which cannot be described in terms of a space and time averaged molecular field alone.

Corrections to quantities calculated in the above-defined Stoner model, which in Ni_3Ga are generally very large for γ, m_c^*, and α, may be described partly in terms of the electron-phonon interaction, but probably mostly in terms of thermally excited enhanced magnetic fluctuations arising essentially from the effect of a molecular field which is *local* in space and time. An analysis of the thermal properties of Ni_3Ga in terms of a quantitative theory of magnetic fluctuations[4,5] which accounts well for the magnetic equation of state of Ni_3Al both in the ferromagnetic and paramagnetic state, and of MnSi in the paramagnetic state at low temperatures, will be presented in a separate paper.

VI. CONCLUSIONS

The main features of the de Haas–van Alphen spectra in Ni_3Ga are found to be in good agreement overall with predictions of our first-principles band model based on the conventional local-spin-density approximation (Table I). At high magnetic fields a slight splitting of the frequency branches associated with bands 14 and 15 is observed which can be understood in terms of the effect of the spin-orbit interaction and an exchange splitting Δ given approximately by $(n_\uparrow-n_\downarrow)/N_F$, i.e., as expected in the Stoner model discussed in Sec. IV B. Strikingly, however, only one frequency branch has been observed which is clearly associated with the $\langle 100\rangle$ neck of sheet 17. Thus in this case the spin splitting of the dHvA frequency is anomalously small or the amplitude of one of the spin split branches is unusually weak. The effect of exchange in this case appears to be quite different from that observed in the more traditional magnetic materials.[20]

While the fundamental frequencies are in close agreement with our paramagnetic band model, the cyclotron masses m_c^*, the linear coefficient of the heat capacity γ, the magnetic susceptibility at low temperatures χ, and the quadratic coefficient α of the inverse susceptibility, are all larger than the band-structure values m_c, γ_0, χ_0, and α_0, respectively (Tables I and III). The high Stoner enhancement factor, $S=\chi/\chi_0\simeq 98$, may perhaps be accounted for approximately in a self-consistent calculation of the bands in the presence of an applied field. However, the strong renormalization of m_c^*, γ, and α cannot be understood in this framework and may point to the importance of enhanced magnetic fluctuations in this system. Our study provides a part of the information required for an analysis, to be presented in a separate paper, of the role of spin fluctuations on the low-temperature properties.

ACKNOWLEDGMENTS

We wish to thank N. R. Bernhoeft, T. I. Sigfusson, and M. Wulff for many helpful discussions in the early stages of this work.

[1]C. J. Schinkel, F. R. de Boer, and B. de Hon, J. Phys. F 3, 1463 (1973).
[2]W. de Dood and P. F. de Chatel, J. Phys. F 3, 1039 (1973).
[3]T. Moriya, J. Magn. Magn. Mater. **31-34**, 10 (1983).
[4]G. G. Lonzarich, J. Magn. Magn. Mater. **45**, 43 (1984); **54-57**, 3A3 (1986).
[5]G. G. Lonzarich and L. Taillefer, J. Phys. C **18**, 4339 (1985).
[6]N. R. Bernhoeft, G. G. Lonzarich, P. W. Mitchell, and D. McK. Paul, Phys. Rev. B **28**, 422 (1983).
[7]T. I. Sigfusson, N. R. Bernhoeft, and G. G. Lonzarich, J. Phys. F **14**, 2141 (1984).
[8]G. G. Lonzarich and N. S. Cooper, J. Phys. F **13**, 2241 (1983).
[9]S. M. Hayden, Ph.D. thesis, University of Cambridge, 1984.
[10]T. I. Sigfusson and G. G. Lonzarich, Phys. Scr. **25**, 720 (1982).
[11]G. G. Lonzarich, Ph.D. thesis, University of British Columbia, 1973.
[12]G. G. Lonzarich and A. V. Gold, Can. J. Phys. **52**, 694 (1974).
[13]J. M. F. Gunn, J. Phys. F **15**, L89 (1985).
[14]O. K. Anderson, Phys. Rev. B **12**, 3060 (1975); H. L. Skriver, *The LMTO Method* (Springer-Verlag, Berlin, 1984).
[15]U. von Barth and L. Hedin, J. Phys. C **5**, 1629 (1972).

[16]J. J. M. Buiting, J. Kubler, and F. M. Mueller, J. Phys. F **13**, L179 (1983).
[17]G. C. Fletcher, Physica **62**, 41 (1972).
[18]J. M. van Ruitenbeek, A. P. J. van Dearsen, L. W. M. Schreurs, R. A. de Groot, A. R. de Vroomen, Z. Fisk, and J. L. Smith, J. Phys. F **14**, 2555 (1984).
[19]F. R. de Boer, C. J. Schinkel, J. Biesterbos, and S. Proost, J. Appl. Phys. **40**, 1049 (1969).
[20]G. G. Lonzarich, *Electrons at the Fermi Surface,* edited by M. Springford (Cambridge University Press, Cambridge, 1980), Chap. 6.
[21]F. Acker, Z. Fisk, J. L. Smith, and C. Y. Huang, J. Magn. Magn. Mater. **22**, 250 (1981).
[22]R. Lamaire, Cobalt **33**, 201 (1966).
[23]Landolt-Börnstein, *Zahlenwerte und Funktionen aus Physik, Chemie, Astronomie, Geophysik und Technik, 6th ed., Band 2, Teil 9, Magnetic Properties I* (Springer-Verlag, Berlin, 1962).